Supporting Information for "The Global Teleconnection Signature of the Madden-Julian Oscillation and its Modulation by the Quasi-Biennial Oscillation"

Benjamin A. Toms[1]*, Elizabeth A. Barnes[1], Eric D. Maloney[1], and Susan C. van den Heever[1]

[1]Department of Atmospheric Science, Colorado State University, Fort Collins, Colorado

Contents

S1: Calculation of RMM for CESM2-WACCM

The process by which RMM was constructed by Wheeler and Hendon (2004) is followed exactly to generate the RMM-like index for CESM2-WACCM, as follows. First, the seasonal cycle of OLR, 850 hPa zonal wind, and 200 hPa zonal wind is removed from each grid point within the tropics (15°S to 15°N) separately by subtracting the mean and first three harmonics of the simulation-long annual cycle. Then, the influences of longer term variability is removed from each field by subtracting a running mean of the previous 120 days. These anomalous time series are then equatorially averaged across the 15°S to 15°N band, which renders time series representing the latitudinal-mean anomalous values of each variable within the tropics throughout the duration of the simulation, for each longitudinal grid point. This process is completed separately for each of the three historical CESM2-WACCM CMIP6 simulations. Thereafter, the time series for each grid point for the three simulations are concatenated together for each variable individually. This generates a single time-space matrix for each variable for each simulation of shape $\{N_{times},N_{longitudes}\}$. The time-space matrices for each variable are then appended together into a single matrix, such that the size of the matrix is now of shape $\{N_{times},3N_{longitudes}\}$. Principal component analysis is then performed on this matrix, the two leading modes of which are the representation of the MJO within CESM2-WACCM.

S2: Removing ENSO Years

We test the dependence of our conclusions on ENSO using two methods. For the first method, the ENSO teleconnection pattern is removed from the 300-hPa geopotential height field by regressing a daily interpolated Oceanic Niño Index (ONI; see *https://origin.cpc.ncep.noaa.gov/products/analysis_monitoring/ensostuff/ONI_v5.php* for details) time series spanning from 1980 through 2016 that has been smoothed with a thirty-day running mean onto the 300-hPa geopotential height field across a similar time span, then subtracting this regressed pattern from the geopotential height time series. This technique is effectively similar to bandpass filtering the extratropical teleconnections to remove teleconnections with periods similar to ENSO, and thereby does not directly consider the impacts of ENSO on the MJO teleconnections. It therefore has little to no effect on the results of our analysis. For the second method, we first

*Department of Atmospheric Science, Colorado State University, 1371 Campus Delivery, Fort Collins, Colorado 80523

Corresponding author: Benjamin A. Toms, ben.toms@colostate.edu

remove all seasons during which a significant ENSO event occurred, which for ONI is defined as a 3-month average of sea-surface temperature anomalies with a magnitude greater than 1 degree Celsius. This method does have the potential to have a direct impact on our analysis, since we reduce the number of samples from which we can estimate the Coh^2.

We also complete the analysis for the observational record, but discard seasons during which a significant ENSO (ONI $>1^{\circ}$) event occurs. These results are shown in Figures S1 and S2. The spatial patterns of the MJO teleconnections for this more direct method of removing the ENSO signal are similar to those when ENSO is not removed, which lends confidence that the ENSO signal does not substantially alter the dependence of MJO teleconnection patterns on the phase of the QBO, at least for the data analyzed in this study.

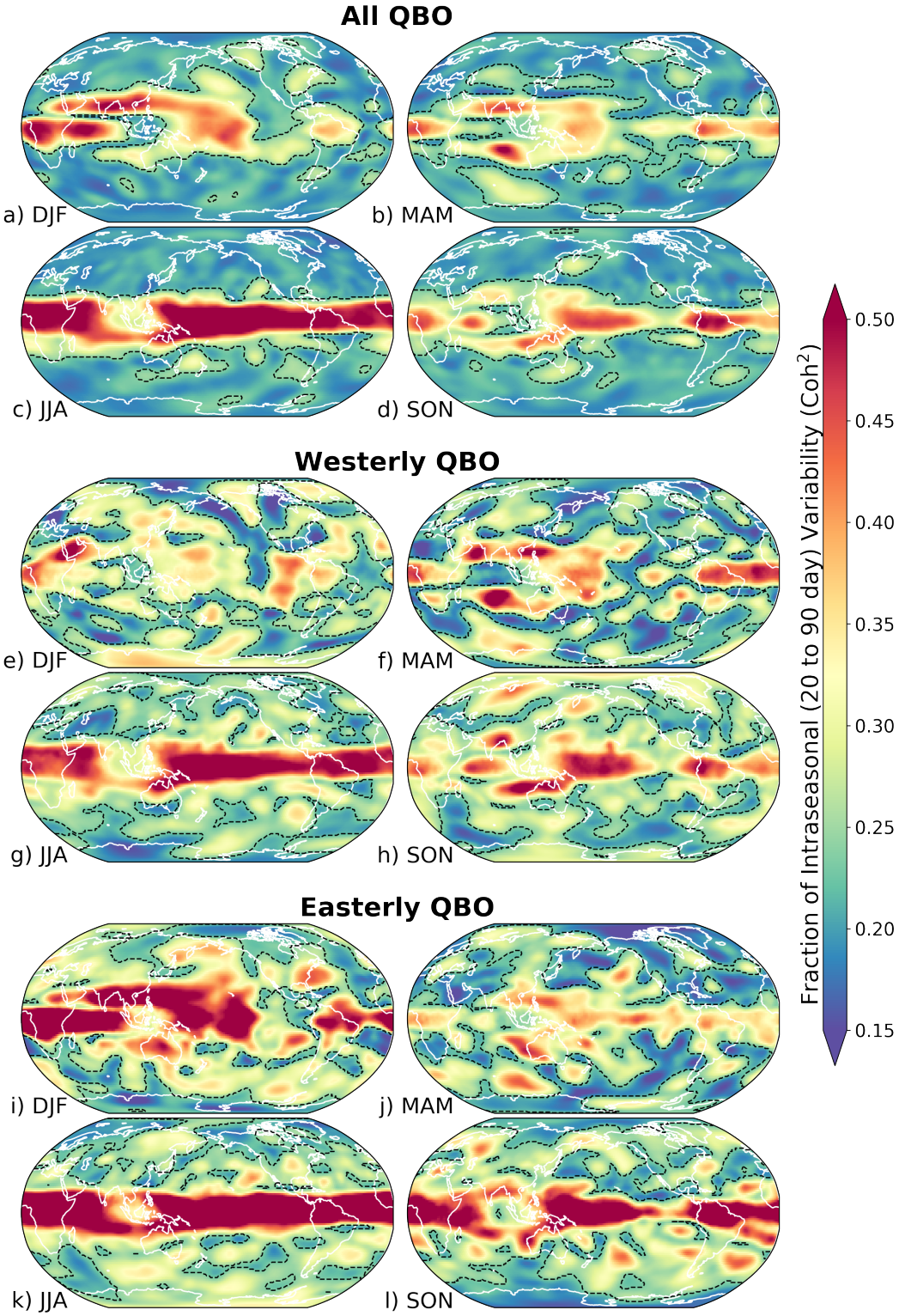

Figure 1. As in Figure 5 of the manuscript, but for the analysis that does not include seasons with significant ENSO activity (ONI >1°C).

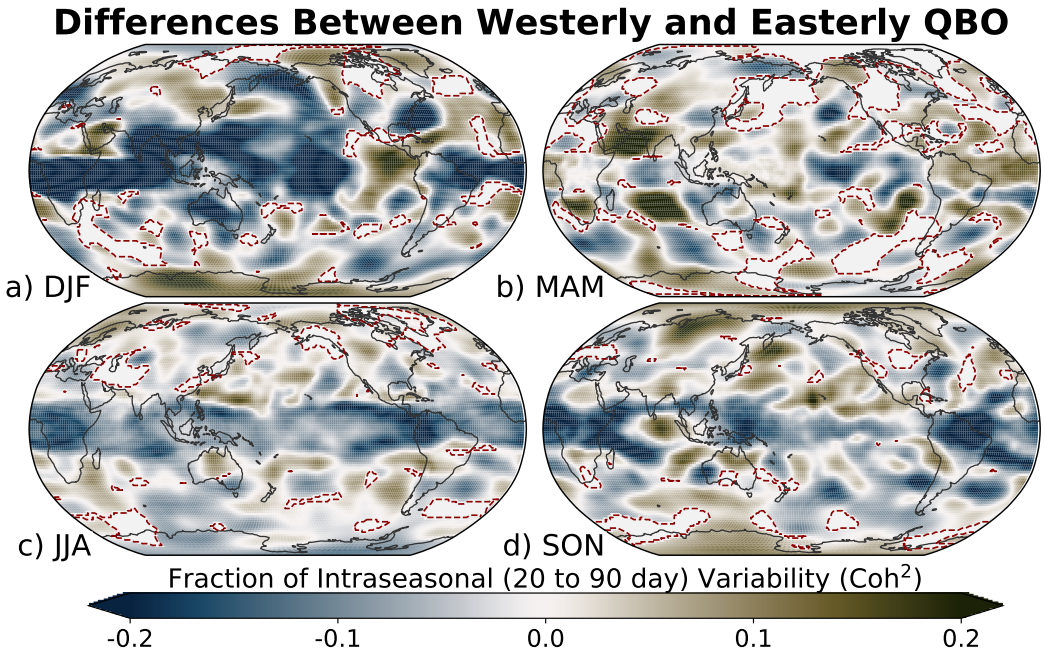

Figure 2. As in Figure 6 of the manuscript, but for the analysis that does not include seasons with significant ENSO activity (ONI >1°C).

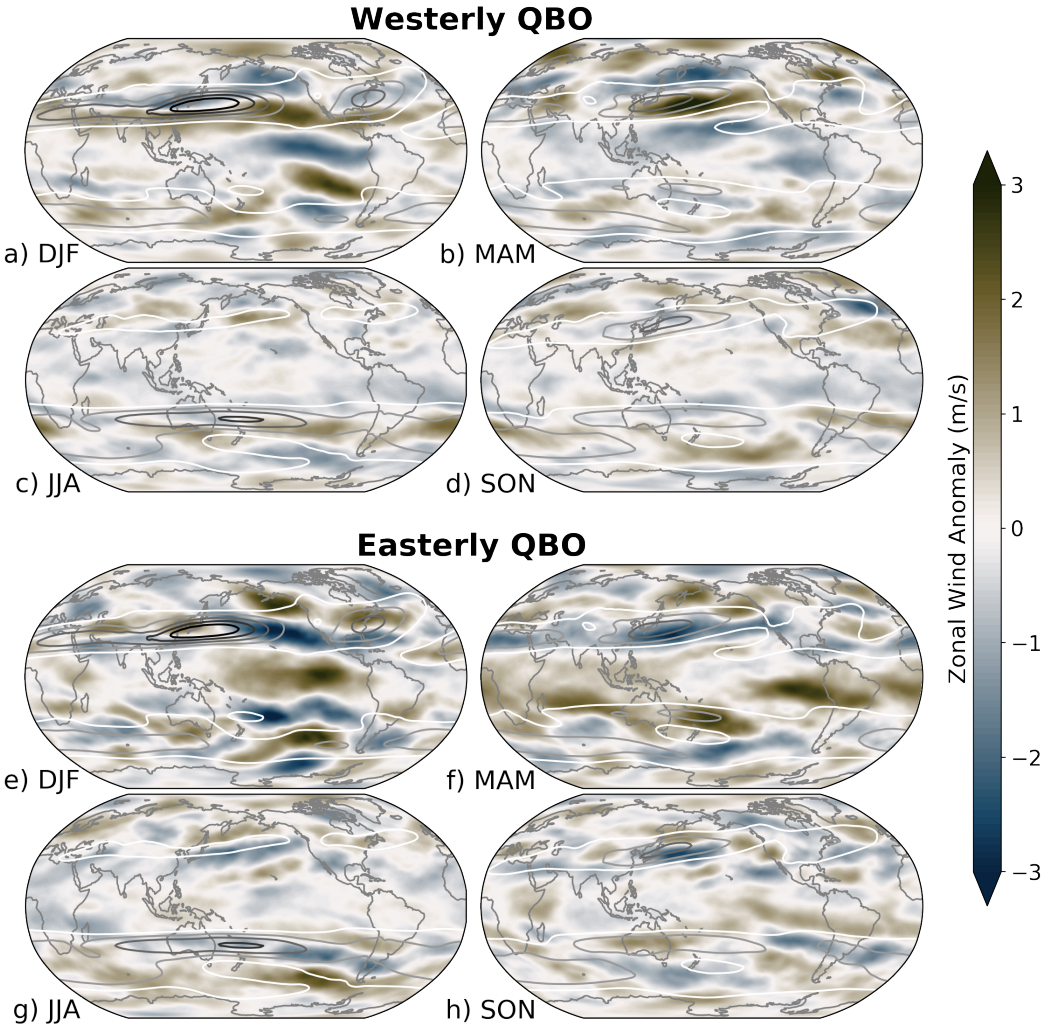

Figure 3. Composite zonal wind characteristics during easterly and westerly QBO phases. The basic state zonal wind composited across all QBO phases is shown in the open contours, with contours of increasing darkness representing the 20, 30, 40, 50, and 60 m s^{-1} thresholds. The anomalies from this all QBO basic state are shown for the westerly QBO (a through d) and easterly QBO (e through h) for all four seasons. Positive (negative) anomalies denote a westerly (easterly) anomaly. Note that the mean zonal wind is westerly within the extratropics and easterly within the tropics (not shown).

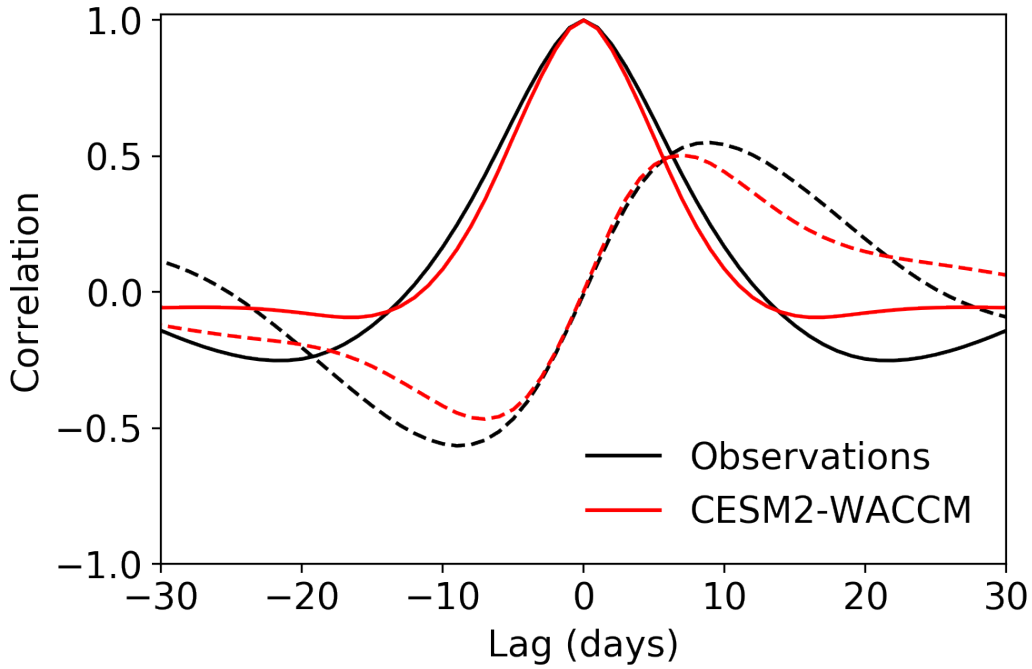

Figure 4. Lagged correlation between the observed RMM1 and itself (solid black) and the observed RMM1 and RMM2 (dashed black). The red lines show the same correlation metrics, but for the correlation of the RMM indices of the modeled MJO in CESM2-WACCM.

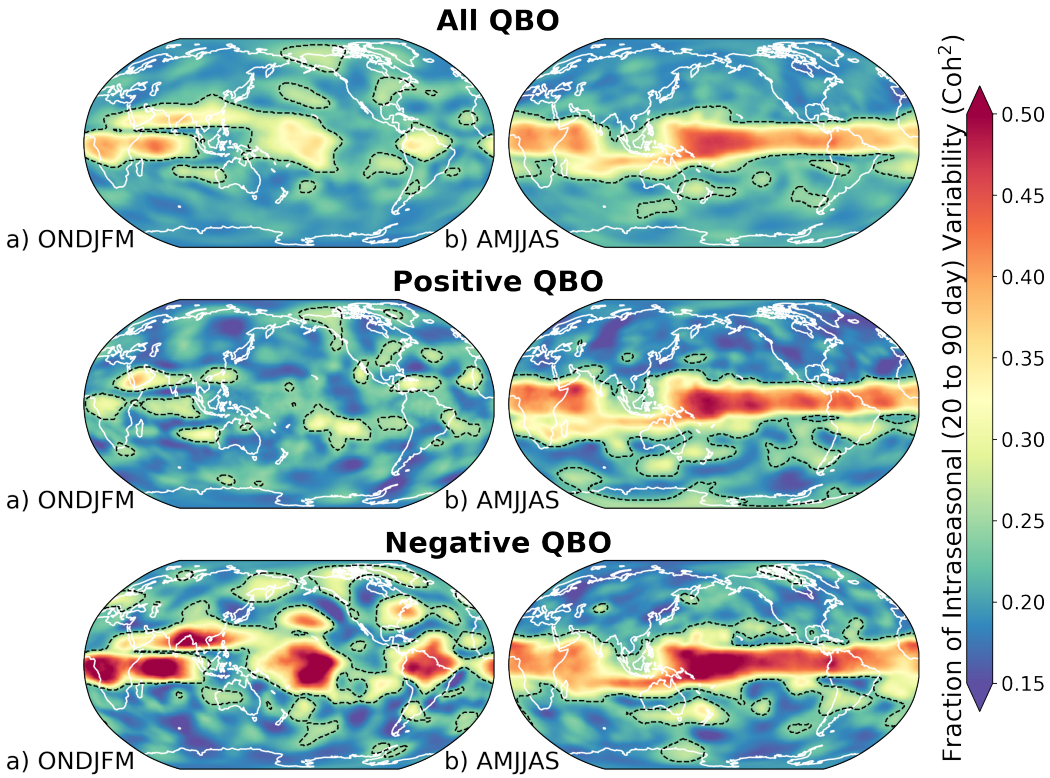

Figure 5. As in Figure 5 of the manuscript, but for the extended season analysis. Here, we only consider the extended boreal winter (ONDJFM) and summer (AMJJAS) seasons.